Progress In Electromagnetics Research Letters, Vol. 41, 29–38, 2013

A NOVEL TUNABLE ANTENNA AT THZ FREQUENCIES USING GRAPHENE-BASED ARTIFICIAL MAGNETIC CONDUCTOR (AMC)

Xu-Chen Wang*, Wen-Sheng Zhao, Jun Hu, and Tian Zhang

Centre for Opt. & EM Research, Zhejiang Provincial Key Lab for Sensing Technologies, State Key Lab of MOI, Zhejiang University, Hangzhou 310058, China

Abstract—In this paper, a novel tunable antenna using graphene-based artificial magnetic conductor (AMC) is proposed and investigated. The resonance frequency of the AMC ground plane can be electrically tuned by applying a gate voltage. A bowtie-shaped antenna is mounted above the 15×15 AMC units. It is observed that the operating frequency of the antenna system shifts in a large range when varying the external electric field. The bandwidth of the antenna system can reach as high as 47% with a gain higher than 9 dB.

1. INTRODUCTION

In recent years, artificial magnetic conductor (AMC) ground plane has been widely used in the design and implementation of high-efficient and low-profile antennas [1–6]. In comparison with perfect electric conductor (PEC) ground plane, the AMC one can significantly reduce the separation distance from the radiator to the ground plane due to the additional capacitance introduced by the periodic pattern. For some antennas based on the modes excited on the surface, the AMC can expand the bandwidth [7]. However, for other applications, especially the ultra-wide bandwidth (UWB) antennas, it may cause severe bandwidth degradation due to its relatively narrowband [1]. To achieve dynamic tuning capacity and broaden the AMC bandwidth, the capacitive lumped elements such as varactor diodes were inserted between the metallic AMC units [1, 3]. In [4], an adjustable air-gap was used in the substrate to attain the frequency band selection,

Received 2 May 2013, Accepted 31 May 2013, Scheduled 9 June 2013

* Corresponding author: Xu-Chen Wang (zjuwangxuchen@163.com).

which can also be realized by adopting magnetic controllable ferrite material instead of traditional dielectric [6]. Nevertheless, at very high frequencies (for example THz), all of the tuning methods mentioned above become unrealistic because of the extremely small sizes of the antennas.

On the other hand, graphene has attracted much attention due to its extraordinary electrical, thermal, mechanical and optical properties [8, 9]. The dynamic variation of its surface conductivity, which can be modulated with an external electric field or chemical doping, makes the tunability of THz devices a reality. In [10], the radiation pattern of dipole antenna array was controlled by switching between the low- and high-resistivity states of graphene ground plane. A beam reconfiguration antenna was designed using a switchable high impedance surface (HIS) [11]. In [12], graphene acts as an antenna radiator and has an active resonance frequency based on the concept of surface plasmonic resonance.

In this work, a novel tunable antenna using graphene-based AMC is proposed for THz applications. With different electric fields applied, the equivalent capacitance of the AMC is changed, and the resonance frequency shifts subsequently. Compared to other tuning structures, the graphene-based AMC can be effective used for nanoscale THz devices and is easy to process. Moreover, it can provide a wider bandwidth than previously proposed models.

2. THE REFLECTION CHARACTERISTICS OF GRAPHENE-BASED AMC

The AMC unit cell made of graphene sheet is shown in Figure 1(a), and the surface impedance of the patch array at THz band can be approximated by [6, 13, 14]

$$Z_g = j\left(\frac{D}{D-g}\frac{1}{\sigma} - \frac{1}{\omega C_{eff}}\right) \tag{1}$$

$$C_{eff} = \frac{1}{\pi}\varepsilon_0\left(\varepsilon_r + 1\right) D \ln\left[\csc\left(\frac{\pi}{2}\frac{g}{D}\right)\right] \tag{2}$$

where D is the period of the square patches, g is the gap between adjacent patches, τ is the relaxation time, ε_r is the relative permittivity of the substrate, and C_{eff} is the capacity related to the patch geometry and background environment. It is known that graphene can be modeled as an infinitesimally thin surface characterized by a surface conductivity $\sigma(\omega, \Gamma, \mu_c, T)$. With the help of Kubo formalism, the Drude model of graphene surface conductivity in intraband can be

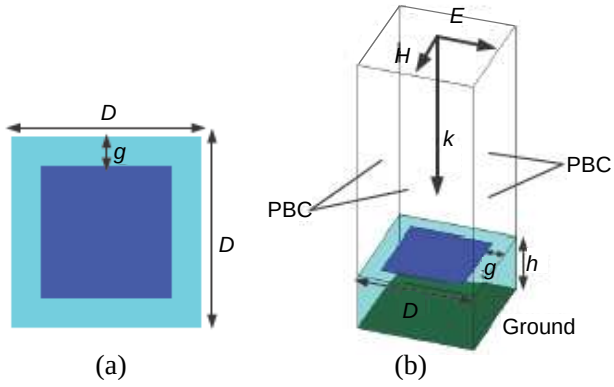

Figure 1. (a) Schematic of AMC unit cell, and its (b) CST model for re ection phase computation with the periodic boundary condition (PBC) adopted.

given by [15]

$$\sigma(\omega) = \sigma_0/(1+j\omega\tau) \tag{3}$$

$$\sigma_0 = \frac{e^2 k_B T\tau}{\pi\hbar^2}\left[\frac{\mu_c}{k_B T} + 2\ln\left(1+e^{-\mu_c/k_B T}\right)\right] \tag{4}$$

where ω is the angular frequency, k_B the Boltzmann's constant, $\hbar$ the reduced Planck's constant, T the temperature, and μ_c the chemical potential of graphene sheet. Throughout this work, we assume $T = 300\,\mathrm{K}$, $\tau = 1\,\mathrm{ps}$, and μ_c is below $1\,\mathrm{eV}$ [16]. The relationship between the electric bias field E and μ_c (see Figure 2) can be calculated by [15]

$$E = \frac{e}{\pi\hbar^2 \upsilon_F \varepsilon_0}\int_0^\infty \varepsilon\left(f_d(\varepsilon) - f_d(\varepsilon+2\mu_c)\right)d\varepsilon \tag{5}$$

where

$$f_d(\varepsilon) = \left(e^{(\varepsilon-\mu_c)/k_B T}+1\right)^{-1} \tag{6}$$

When $\omega\tau \gg 1$, the grid impedance can be approximated as a pure reactance, and $Z_g^{\omega\tau\gg1} = (j\omega C_g(\omega))^{-1}$, where $C_g(\omega)$ is the equivalent capacitance of the grid pattern.

According to the transmission line theory, the impedance of the grounded substrate for normal incident wave can be written as

$$Z_d = j\eta_0 \tan(k_d h)/\sqrt{\varepsilon_r} = j\omega L_d(\omega) \tag{7}$$

where η_0 is the wave impedance in free space, h is the substrate thickness, k_d $(= \omega\sqrt{\mu_0\varepsilon_0\varepsilon_r})$ is the wave number of the incident wave

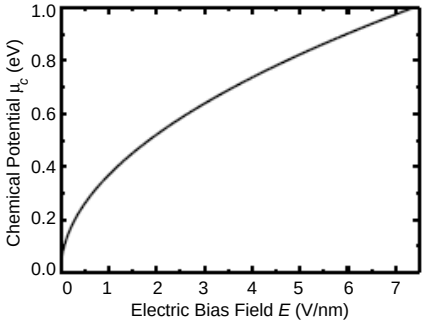

Figure 2. The relationship between the electric bias field and chemical potential.

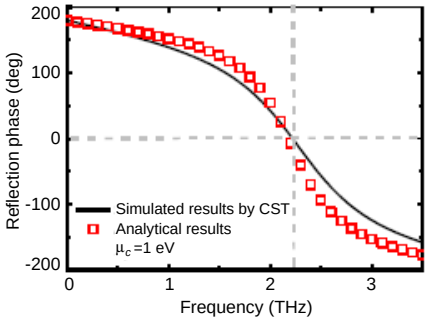

Figure 3. Comparison between theoretical and simulated reflection phase for transverse electric (TE)-polarized incident wave when $\mu_c = 1\,\text{eV}$.

in substrate, and $L_d(\omega)$ is the equivalent inductance of the grounded substrate.

The total surface impedance is a parallel combination of capacitance grid impedance of the array and inductive impedance of the grounded substrate [13]

$$Z_s = Z_g Z_d/(Z_g + Z_d) \tag{8}$$

As shown in Figure 1(b), the reflection phase R can be computed using a normally incident TE wave by

$$\mathrm{R} = (Z_s - \eta_0)/(Z_s + \eta_0) \tag{9}$$

A comparison of the reflection phase obtained by analytical equations and simulation is shown in Figure 3, and good agreement is obtained.

Here, the impact of chemical potential μ_c on the resonance frequency of AMC surface is investigated in detail. As shown in Figure 4(a), a maximum shift of 0.75 THz (from 1.47 to 2.22 THz) can be achieved in the resonance frequency of AMC surface by varying μ_c from 0.15 to 1 eV. In addition, the tuning capacity at low μ_c is more effective than that at high one. As μ_c increases, the phase curve becomes more flat, which means an improved bandwidth. To explain this phenomenon, Figure 5 shows the equivalent circuit model of AMC surface, and its input impedance is inductive as the substrate thickness is much smaller than the wavelength [13]. Therefore, the resonance frequency of AMC surface can be expressed as

$$\omega_0 = 1\Big/\sqrt{C_g L_d} \tag{10}$$

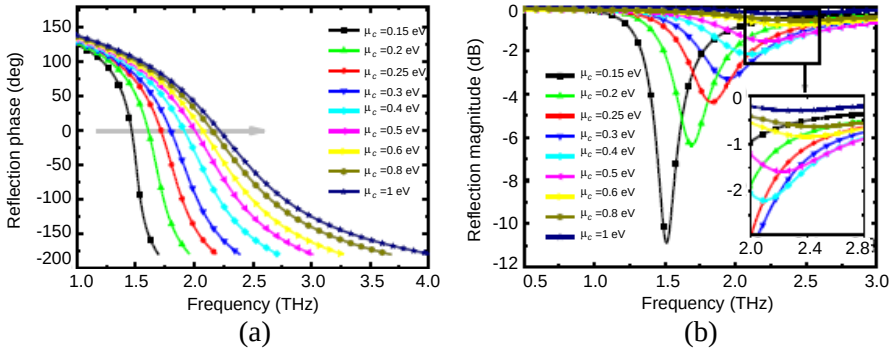

Figure 4. The reflection (a) phase and (b) magnitude of the AMC surface obtained by commercial software CST.

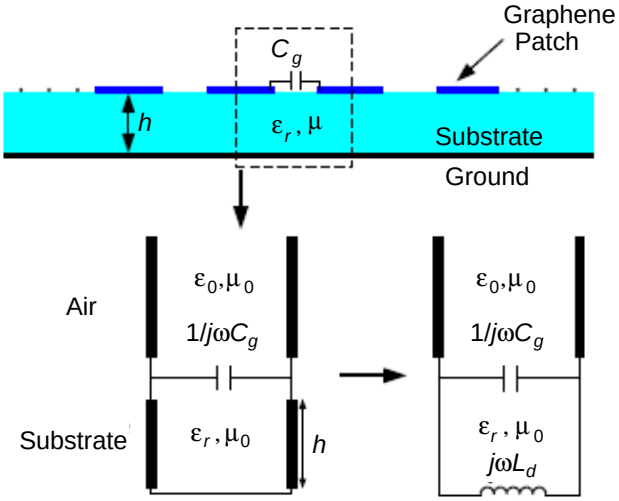

Figure 5. The equivalent circuit model of the AMC surface.

The bandwidth of AMC is defined as the frequency range when its reflection phase changes from $+90^\circ$ to -90°, and is proportional to $\sqrt{L_d/C_g}$. As μ_c increases, the grid impedance becomes less capacitive, and therefore, both the resonance frequency and bandwidth increase. Figure 4(b) shows the reflection magnitude of the AMC surface, and its minimum value is about -11 dB. The AMC ground plane becomes more reflective as μ_c increases, which is caused by the mushroomed carrier concentration and ensuing ohmic loss in graphene patches. However, when $\mu_c < 0.15$ eV, the ohmic loss in graphene becomes severe and the reflection magnitude drops rapidly. Under such circumstances, the graphene patch array should be viewed as an

absorber rather than the AMC ground plane. Note that the spatial dispersion may significantly affect the waves excited on graphene transferred onto a dielectric, as demonstrated in [17]. However, it may not be important in our work due to the large μ_c and the relatively low ε_r of the substrate employed in our simulation. In addition, the current full-wave simulators cannot take this phenomenon into account, so the spatial dispersion is excluded in this work.

3. ANTENNA MODEL AND CHARACTERIZATION

In this section, a simple bowtie antenna made of Cu is placed above the graphene-based AMC ground plane, as shown in Figures 6(a) and (b). The potential fabrication strategy is briefly introduced as follows. A 10-μm-thick grounded SiO_2 is employed as the AMC substrate. In consideration of the feasibility in fabrication, a 300-μm-thick silicon handle wafer is bounded under the quartz substrate. Above the quartz is a 50-nm-thick polycrystalline silicon layer and 10-nm-thick Al_2O_3 film in sequence, which can be easily obtained by RF sputtering. The AMC ground plane consists of 15×15 graphene square patches with $D = 10, \mu m$ and $g = 1\,\mu m$, which can be patterned by high resolution e-beam lithography tool. The graphene patches can be connected by 60-nm-wide graphene nano-ribbons (GNR) to keep all patches at the same μ_c when applying a DC voltage between the AMC and polycrystalline silicon [18, 19]. The GNRs are excluded in our simulation due to their negligible impact on the whole device. Using the chemical vapor deposition (CVD), a 2-μm-thick SiO_2 is deposited on graphene-based AMC, and the gold antenna can be finally fabricated by photolithography method.

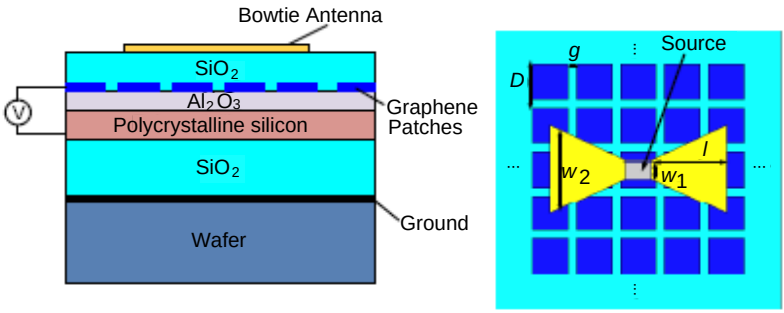

Figure 6. The (a) side and (b) top views of our proposed antenna system. Here, $D = 10\,\mu m$, $g = 1\,\mu m$, $w_1 = 4\,\mu m$, $w_2 = 20\,\mu m$, and $l = 24\,\mu m$.

The original resonance frequency of the bowtie antenna is optimized to be 2 THz. Figures 7(a)–(d) show the return loss of the antenna system (including the bowtie antenna and graphene-based AMC ground plane) at different μ_c. It is obvious that the operating frequency of the antenna will be greatly influenced when the active AMC is introduced. The best matched frequency point of the antenna system is always close to the resonance frequency of the AMC. At $\mu_c = 0.25$ eV, the bandwidth of the antenna system is 11% (0.37 THz), which is smaller than that of the original bowtie antenna. However, with the increase of μ_c, the AMC bandwidth increases and the antenna system can be best matched at several frequencies, which will expand its bandwidth greatly (from 22% to 47%). Therefore, by varying the applied voltage, the operating frequency of the antenna system shift from 1.45 to 3.21 THz.

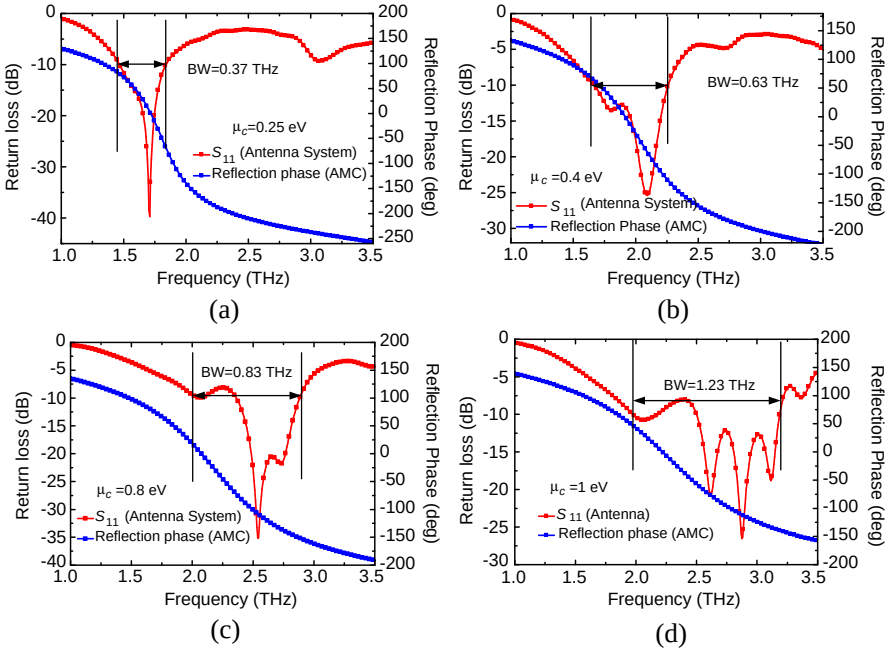

Figure 7. The return loss of bowtie antenna placed above the graphene-based AMC at different μ_c. (a) μ_c=0.25 eV. (b) μ_c=0.4 eV. (c) μ_c=0.8 eV. (d) μ_c=1 eV.

Figures 8(a) and (b) show the gain patterns of the bowtie antenna with and without ground plane, respectively. The maximum gain of the antenna system is about 9.19 dB, which is much larger than that of the bowtie antenna without the ground plane. Obviously, both the

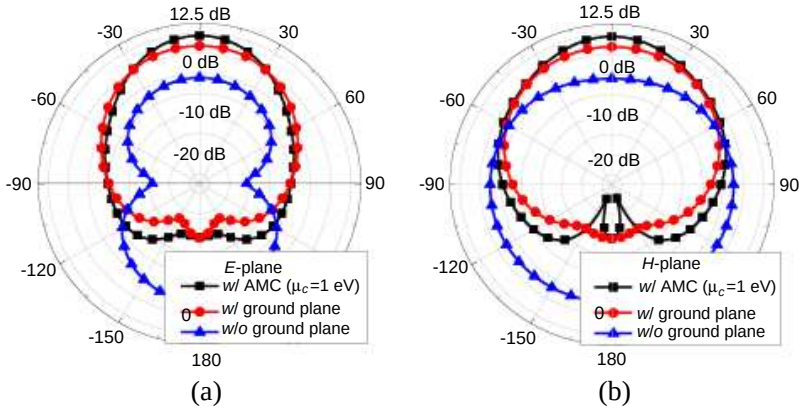

Figure 8. Gain patterns of the bowtie antenna with and without the ground plane. (a) E-plane. (b) H-plane.

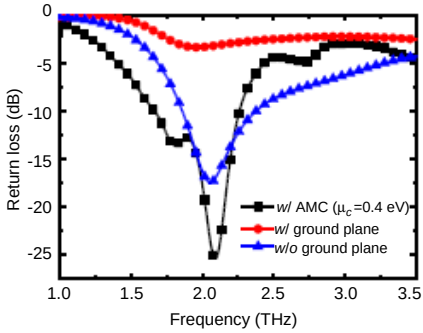

Figure 9. Return loss of the bowtie antenna with and without the ground plane.

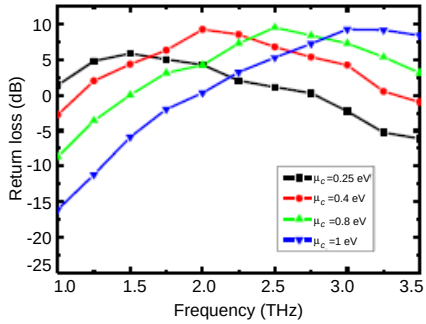

Figure 10. The maximum gain of the antenna placed above graphene-based AMC at different μ_c.

traditional and AMC ground planes can significantly improve the gain. However, the traditional ground plane leads to mismatch, as shown in Figure 9. Further, the gain of the antenna system at different μ_c is plotted in Figure 10. It is found that the maximum gain reaches its peak value near the resonance frequency of AMC and decreases when deviating from this frequency.

4. CONCLUSION

In this paper, a novel tunable low-profile antenna is developed. First, the tunability of a graphene-based AMC is demonstrated by varying

its chemical potential. It is shown that both the resonance frequency and bandwidth increases with the applied voltage. Then, the bowtie antenna is mounted above the graphene-based AMC ground plane to form the whole tunable antenna system. The operating frequency of the antenna system can be tuned from 1.45 to 3.21 THz when adjusting the chemical potential from 0.25 to 1 eV. Remarkable improvement of the gain can be observed, which has the peak value larger than 9 dB.

ACKNOWLEDGMENT

This work was supported by the Program of Zhejiang Leading Team of Science and Technology Innovation.

REFERENCES

1. Bray, M. G. and D. H. Werner, "A broadband open-sleeve dipole antenna mounted above a tunable EBG AMC ground plane," *Int. Symp. Antennas Propag. Society*, Vol. 2, No. 10, 1147–1150, 2004.
2. Hu, J., C. S. Yan, and Q. C. Lin, "A new patch antenna with metamaterial cover," *J. Zhejiang Univ. Sci. A*, Vol. 7, No. 1, 89–94, 2006.
3. Costa, F., S. Talarico, A. Monorchio, and M. F. Valeri, "An active AMC ground plane for tunable low-profile antenna," *Int. Symp. Antennas Propag. Society*, 1–4, San Diego, CA, 2008.
4. Veysi, M. and M. Shafaee, "EBG frequency response tuning using an adjustable air-gap," *Progress In Electromagnetics Research Letters*, Vol. 19, 31–39, 2010.
5. Zhao, L., D. Yang, H. Tian, Y. Ji, and K. Xu, "A pole and AMC point matching method for the synthesis of HSF-UC-EBG structure with simultaneous AMC and EBG properties," *Progress In Electromagnetics Research*, Vol. 133, 137–157, 2013.
6. Padooru, Y. R., A. B. Yakovlev, C. S. R. Kaipa, G. W. Hanson, F. Medina, and F. Mesa, "Dual capacitive-inductive nature of periodic graphene patches: Transmission characteristics at low-terahertz frequencies," *Phys. Rev. B*, Vol. 87, 115401, 2013.
7. Cook, B. S. and A. Shamim, "Utilizing wideband AMC structures for high-gain inkjet-printed antennas on lossy paper substrate," *IEEE Antennas Propag. Wireless Lett.*, Vol. 12, 76–79, 2013.
8. Geim, K. and K. S. Novoselov, "The rise of graphene," *Nat. Mater.*, Vol. 6, 183–191, 2007.
9. Hotopan, G. R., S. Ver-Hoeye, C. Vazquez-Antuna, R. Camblor-Diaz, M. G. Fernandez, F. Las Heras Andres, P. Alvarez,

and R. Menéndez, "Millimeter wave microstrip mixer based on graphene," *Progress In Electromagnetics Research*, Vol. 118, 57–69, 2011.

10. Dragoman, M., A. A. Muller, D. Dragoman, F. Coccetti, and R. Plana, "Terahertz antenna based on graphene," *J. Appl. Phys.*, Vol. 107, 104313, 2010.
11. Huang, Y., L. S. Wu, and J. F. Mao, "Design of a beam reconfigurable THz antenna with graphene-based switchable high-impedance surfaces," *IEEE Trans. on Nanotechnol.*, Vol. 11, No. 4, 836–842, 2012.
12. Tamagnone, M., J. S. Gómez-Díaz, J. R. Mosig, and J. Perruisseau-Carrier, "Reconfigurable terahertz plasmonic antenna concept using a graphene stack," *Appl. Phys. Lett.*, Vol. 101, No. 21, 214102, 2012.
13. Tretyakov, S., *Analytical Modeling in Applied Electromagnetics*, Artech House, Inc., 2003.
14. Luukkonen, O., C. Simovski, G. Granet, G. Goussetis, D. Lioubtchenko, A. V. Raisanen, and S. A. Tretyakov, "Simple and accurate analytical model of planar grids and high-impedance surfaces comprising metal strips or patches," *IEEE Trans. on Antennas Propag.*, Vol. 56, No. 6, 1624–1632, 2008.
15. Hanson, G. W., "Dyadic Green's functions for an anisotropic, non-local model of biased graphene," *IEEE Trans. on Antennas Propag.*, Vol. 56, No. 3, 747–757, 2008.
16. Bolotin, K. I., K. J. Sikes, Z. Jiang, M. Klima, G. Fudenberg, J. Hone, P. Kim, and H. L. Stormer, "Ultrahigh electron mobility in suspended graphene," *Solid State Commun.*, Vol. 146, 351–355, 2008.
17. Lovat, G., P. Burghignoli, and R. Araneo, "Low-frequency dominant-mode propagation in spatially dispersive graphene nanowaveguides," *IEEE Trans. Electromagn. Compat.*, Vol. 55, No. 2, 328–333, 2013.
18. Cui, J. P., W. S. Zhao, W. Y. Yin, and J. Hu, "Signal transmission analysis of multilayer graphene nano-ribbon (MLGNR) interconnects," *IEEE Trans. on Electromagn. Compat.*, Vol. 54, No. 1, 126–132, 2012.
19. Carrasco, E., M. Tamagnone, and J. Perruisseau-Carrier, "Tunable graphene reflective cells for THz reflectarrays and generalized law of reflection," *Appl. Phys. Lett.*, Vol. 102, No. 10, 104103, 2013.